Carbohydrate-Modified Magnetic Nanoparticles for Radical Scavenging

M. MOSKVIN[1], D. HORÁK[1]

[1]Institute of Macromolecular Chemistry of the Czech Academy of Sciences, Prague, Czech Republic

Summary

Maghemite (γ-Fe$_2$O$_3$) nanoparticles, 12 nm in size, were prepared by co-precipitation of Fe(II) and Fe(III) chlorides with ammonium hydroxide and oxidation with hydrogen peroxide. To achieve stability and biocompatibility, obtained particles were coated with silica, to which glucose and ascorbic acid were bound by different mechanisms. The composite particles were thoroughly characterized by transmission electron microscopy, dynamic light scattering, elemental analysis, and FT-Raman and fluorescence spectroscopy to determine composition, morphology, size and its distribution, ζ-potential, and scavenging of peroxyl and hydroxyl radicals. As the particles showed promising antioxidative properties, they may have a possible application as a stable magnetically controlled scavenger of reactive oxygen species.

Corresponding author

D. Horák, Institute of Macromolecular Chemistry of the Czech Academy of Sciences, Heyrovského nám. 2, 162 06 Prague 6, Czech Republic. E-mail: horak@imc.cas.cz

Introduction

Naturally occurring carbohydrates and glycoconjugates (glycoproteins and glycolipids) play a crucial role in many diagnostic processes, such as recognition of antigens, cells, and their fragments (Olden *et al.* 1982). Carbohydrates are biocompatible, hydrophilic (mostly water-soluble), and can trigger various biological events including cell growth, inflammatory responses, or viral infections. These useful properties can be conveniently transferred on the glycosylated core-shell conjugates based on superparamagnetic nanoparticles. Such cores offer superior magnetic targetability and manipulability, and/or traceability in magnetic resonance imaging (MRI) due to the fact that iron oxides provide the targeted molecule with a large magnetic moment that creates substantial disturbances in the local magnetic field, leading to a rapid dephasing of water protons (Bulte and Kraitchman 2004). Besides applicability in drug delivery and sensing systems, magnetic nanoparticles are used also in treatment of cancer by hyperthermia (Wust *et al.* 2006). For cell labeling, crucial requirements consist in preparation of water-dispersible monocrystalline iron oxide nanoparticles, which are not only superparamagnetic, but also biocompatible, surface-functionalizable, and at the same time internalized by the cells. MR diagnostics of liver and spleen is their main application field as the particles with size <50 nm are readily and almost completely internalized by the macrophages of these organs (Ferrucci and Stark 1990).

One of the key factors in the design of the magnetic nanoparticles for nanomedical applications is control of the size distribution, because the polydisperse particles differ in physical, chemical, and biological properties, in contrast to the monodisperse ones, the properties of which are uniform. A drawback of majority of iron oxide nanoparticles is that they consist of magnetite (Fe$_3$O$_4$), which loses its properties in the presence of air oxygen. Due to the uncontrolled oxidation, magnetic properties are deteriorating; the colloid loses its stability and forms aggregates, which is unacceptable from the biomedical point of view. Therefore, controlled oxidation of Fe$_3$O$_4$ with hydrogen peroxide or sodium hypochlorite immediately after the synthesis is preferred resulting in maghemite (γ-Fe$_2$O$_3$)

(Babič *et al.* 2008), that is more stable in air and does not change its properties as quickly as the magnetite does (Sun *et al.* 2004). Moreover, Fe^{3+} ions of maghemite can be utilized for chelating bioactive compounds (Kraemer 2004). In contrast, Fe^{2+} ions of magnetite are known to catalyze decomposition of hydrogen peroxide in the cells forming $HO^{\bullet}$ radicals (Fenton reaction (Winterbourn 1995)) and can be toxic in high concentrations.

Biological applications require functionalized particles with inaccessible surface Fe ions. Magnetite/dextran conjugates (GastroMARK®, Endorem®) were the first commercially developed contrast agents approved for oral or intravenous introduction for magnetic resonance imaging (MRI) of bowels or liver (Wang 2011). Dextran, however, decomposes in acidic and alkaline media and cellular uptake of dextran-coated particles does not allow precise MR imaging due to the relatively poor endocytosis (Wilhelm *et al.* 2003).

Another class of surface-modified iron oxides is represented by γ-Fe_2O_3&SiO_2 core-shell (Lu *et. al.* 2002) and/or carbohydrate-coated particles (Dorniani *et al.* 2012). While immobilization chemistry of polysaccharides is relatively simple, direct binding of mono-, di-, and oligosaccharides to iron oxide particles is rather difficult employing, e.g. reaction of aldehyde groups of reduced mono- and disaccharides with hydrazide groups of the particles (Lemieux and Bertozzi 1998). Another well-known approach consists in reductive amination of saccharides with amino group-containing supports (Gildersleeve *et al.* 2008, Geetha *et al.* 1995). Also carbohydrate-derived and especially polyprotic acids (glucuronic (Roque *et al.* 2009), ascorbic (Plug *et al.* 1984), D-gluconic (Kekkonen *et al.* 2009), hyaluronic (Kamat *et al.* 2010) and tannic (Iffat *et al.* 2005)) can be efficiently bound to the iron oxide surface by chemisorption. Due to formation of strong complexes, the acids are then firmly attached to the surface by ionic bonds. Last but not least, certain carbohydrate derivatives possessing antioxidative properties are useful as effective scavengers of reactive oxygen species (ROS). Aim of this report is to demonstrate possible enhancement of colloidal stability and scavenging activity of γ-Fe_2O_3 particles after their surface functionalization with glucose and ascorbic acid.

Materials and Methods

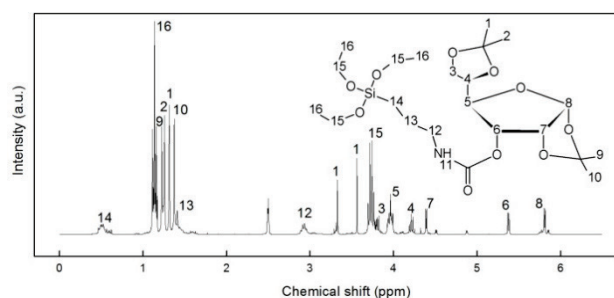$FeCl_2 \cdot 4\ H_2O$, $FeCl_3 \cdot 6\ H_2O$, ascorbic acid (ASA), (3-isocyanatopropyl)triethoxysilane (ITS), 2,2'-azobis(2-amidinopropane) dihydrochloride (AAPH), 3,5-di-*tert*-butyl-4-hydroxytoluene (BHT), tetramethoxyorthosilicate (TMOS), diacetonide of D-glucose (DAG), and dexpanthenol (DXP) were obtained from Sigma-Aldrich (St. Louis, USA). Ethanol, *N,N*-dimethylformamide (DMF), propan-2-ol, 1,4-dioxane, cyclohexanol, iodine, and $Na_2WO_4 \cdot 2\ H_2O$ were from Lachema (Brno, Czech Republic). Hydrochloric acid (35 %), ammonium hydroxide (25 %), hydrogen peroxide (30 %), sodium bicarbonate and fluorescein were obtained from Lach-Ner (Neratovice, Czech Republic). Ultrapure Q-water from a Milli-Q Gradient A10 system (Millipore, Molsheim, France) was used throughout the experiments. All other reagent grade chemicals were purchased from Sigma-Aldrich and used as received.

Preparation of γ-Fe_2O_3 colloid

γ-Fe_2O_3 nanoparticles were prepared according to the previously developed technique (Patsula *et al.* 2016). Briefly, 0.3 M $FeCl_3$ (40 mmol) and 1 M $FeCl_2$ aqueous solutions (20 mmol; Fe^{3+}/Fe^{2+}=2 mol/mol) were charged in a 500-ml glass reactor equipped with a turbine impeller and the mixture was heated to 70 °C with stirring (600 rpm). 25 wt.% NH_4OH (35 ml) was added to the mixture (Fe^{3+}&Fe^{2+}/NH_4OH=5 v/v), magnetite was precipitated and the reaction mixture heated to 90 °C for 1 h with stirring (600 rpm). After cooling to room temperature, 35 % HCl was added to adjust pH to 5-6. Resulting Fe_3O_4 was oxidized to γ-Fe_2O_3 by adding 30 % H_2O_2 (5 ml; Fe^{3+}&Fe^{2+}/H_2O_2=1.2 mol/mol) under slow heating from 20 to 90 °C; reaction continued for 1 h with stirring (550 rpm). Finally, the γ-Fe_2O_3 particles were washed three times with water (100 ml each) and magnetically separated. Particles were dispersed in water (100 ml) under sonication (W-385 Heat Systems-Ultrasonics; Farmingdale, NY, USA) at 50 % output and 50 % duty cycle for 10 min. Concentration of the particles was 45 mg/ml.

Preparation of 5-(2,2-dimethyl-1,3-dioxolan-4-yl)-2,2-dimethyltetrahydrofuro[2,3-d][1,3]dioxol-6-yl (3-(tri-ethoxysilyl)propyl)carbamate (DFSC)

ITS and DAG (2 mmol of each) were dissolved in dry 1,4-dioxane (20 ml) at 70 °C for 6 h with magnetic stirring (600 rpm). 1,4-dioxane was vacuum-distilled off and the resulting DFSC was washed twice with cyclohexanol and vacuum-dried at 40 °C. Structure of DFSC was confirmed by ^{1}H NMR (Fig. 1) using a Bruker Avance 300 MHz spectrometer (Billerica, MA, USA).

Fig. 1. ^{1}H NMR spectrum of DFSC.

Modification of γ-Fe$_2$O$_3$ nanoparticle surface

γ-Fe$_2$O$_3$ was modified in three steps with (i) SiO$_2$, (ii) DFSC, and (iii) ASA.

(i) Typically, in a 25-ml glass reactor equipped with a turbine impeller, TMOS (20 mg) in propan-2-ol/water (8/1 v/v) solution was added to aqueous γ-Fe$_2$O$_3$ colloid (100 mg of dry substance) to reach 25 ml volume and pH was adjusted to 9 by addition of 25 % NH$_4$OH. The mixture was heated to 60 °C for 8 h with stirring (500 rpm). Resulting γ-Fe$_2$O$_3$&SiO$_2$ nanoparticles Run I/1 (Table 1) were washed with water three times (70 ml each), magnetically separated and again dispersed in water (20 ml) under sonication at 50 % output for 3 min.

(ii) γ-Fe$_2$O$_3$&SiO$_2$ particles Run I/1 (100 mg) were coated with D-glucose by adding different amounts of DFSC (10, 20, 50, 100, and 200 mg) as described above. Hydroxyl groups of the resulting γ-Fe$_2$O$_3$&SiO$_2$-DAG particles were deprotected by addition of 0.1 wt.% iodine in methanol under reflux (50 °C) for 8 h with stirring (500 rpm). Resulting glucose-containing γ-Fe$_2$O$_3$&SiO$_2$-G particles Run I/2-6 (Fig. 4) were washed with methanol and water (twice each) and transferred in water with sonication.

(iii) Finally, ASA was adsorbed on the γ-Fe$_2$O$_3$&SiO$_2$-G particles Run I/3 from aqueous solutions at different ASA/γ-Fe$_2$O$_3$&SiO$_2$-G ratios (0.1-2 w/w) under purging with argon. Resulting γ-Fe$_2$O$_3$&SiO$_2$-G-ASA nanoparticles Run II/1-5 were washed with water with sonication; concentration was adjusted to 4.4 mg γ-Fe$_2$O$_3$&SiO$_2$-G-ASA/ml.

Determination of free-radical scavenging

To measure scavenging ability of peroxyl radicals (ROO$^\bullet$), the γ-Fe$_2$O$_3$&SiO$_2$-G-ASA particles (2, 4, 8, and 16 mg) were added to $2.4 \cdot 10^{-5}$ M fluorescein solution in 0.02 M sodium bicarbonate buffer (SBB; 2 ml; pH=7.4) and DMF (1 ml). After addition of freshly prepared AAPH (30 mg) solution in 0.16 M SBB (3 ml),

the radicals were formed and fluorescence spectrum measured for 1 h using a JASCO FP-6200 spectrofluorometer (Tokyo, Japan); each experiment was performed in triplicate and BHT was used as a positive control. Relative scavenging activity A' (%) of the particles was evaluated according to the following formula (1):

$$A' = 100 \cdot (I \cdot K - I_0)/(1 - I_0) \qquad (1),$$

where I_0 and I are relative fluorescence intensities of the blank (without the particles) and particle dispersion, respectively, measured 30 min after beginning of the experiment and K is factor taking in account light scattering by the particles. Absolute scavenging activity A (mmol/g) was calculated according to equation (2):

$$A = [2 \cdot A' \cdot \omega]/[10 \cdot M] = 1.136 \cdot 10^{-3} \cdot A' \cdot \omega \qquad (2),$$

where ω is content of ASA in the particles (wt.%) and M is molar mass of ASA (176.1 g/mol).

To evaluate scavenging activity of the hydroxyl radicals (HO$^\bullet$), the particles (1, 2, 4, 6, and 12 mg) were added to $2.4 \cdot 10^{-5}$ M fluorescein solution (10 µl). Subsequently, 7.3 mM Na$_2$WO$_4$ solution in SBB (20 µl) and 30 % H$_2$O$_2$ (100 µl) were added. Fluorescence of the colloid was monitored for 1.5 h; each experiment was performed in duplicate and DXP was used as a positive control. The particle scavenging activity was evaluated 1 h after beginning of the experiment.

Characterization of particles

Maghemite nanoparticles were observed by a Tecnai Spirit G^2 transmission electron microscope (TEM; FEI; Brno, Czech Republic). Number-average diameter ($D_n = \Sigma D_i/N$, D_i is diameter of i-th particle and N is total number of the particles), weight-average diameter ($D_w = \Sigma D_i^4/\Sigma D_i^3$) and polydispersity index (PDI=D_w/D_n) were calculated from at least 300 individual particles on the micrographs using Atlas software (Tescan Digital Microscopy Imaging; Brno, Czech Republic). Surface zeta (ζ) potential and hydrodynamic diameter D_h were measured by dynamic light scattering (DLS) using a ZEN3600 Nano-ZS Zetasizer (Malvern Instruments; Malvern, Worcestershire, UK). FT-Raman spectra were measured on a Thermo Nicolet 6700 FT-IR spectrometer with attached NIR FT-Raman module (Thermo Fisher Scientific; Waltham, USA). Excitation laser with the 180° reflecting sample geometry and 1,064 nm wave-
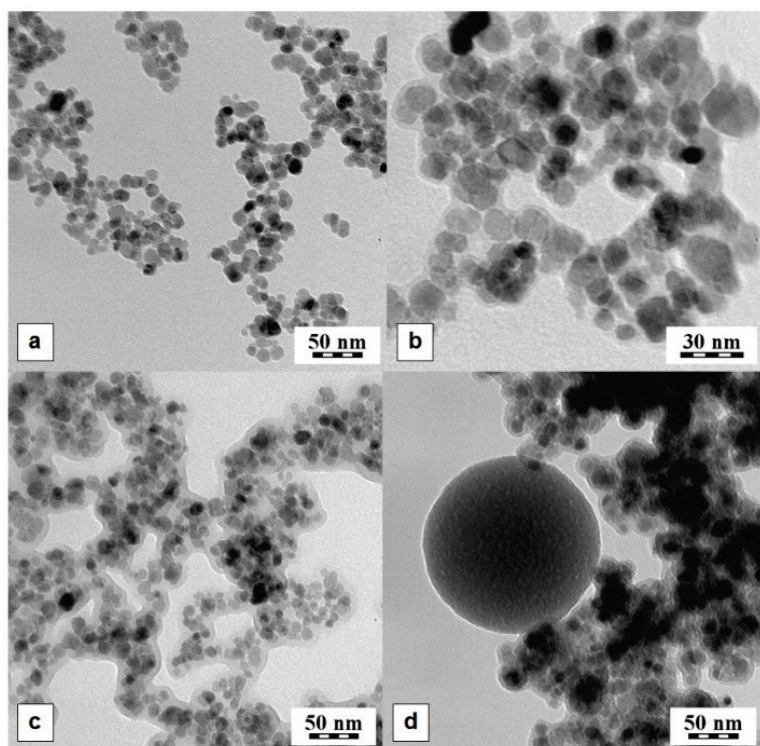
length was used in pair with air-cooled In-Ga-As detector. Carbon and nitrogen content was determined on a Perkin-Elmer 2400 CHN elemental analyzer (Waltham, MA, USA).
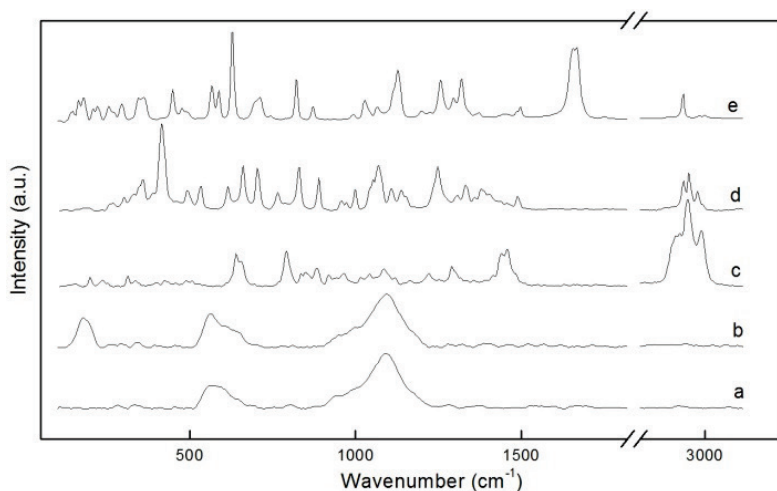
Results

Synthesis of γ-Fe₂O₃ nanoparticles

γ-Fe_2O_3 nanoparticles were obtained by co-precipitation of $FeCl_2$ and $FeCl_3$ with ammonia and oxidation with hydrogen peroxide (Fig. 4). Figure 2a shows TEM micrograph of γ-Fe_2O_3 nanoparticles, that are almost spherical in shape with a mean diameter of 12 nm
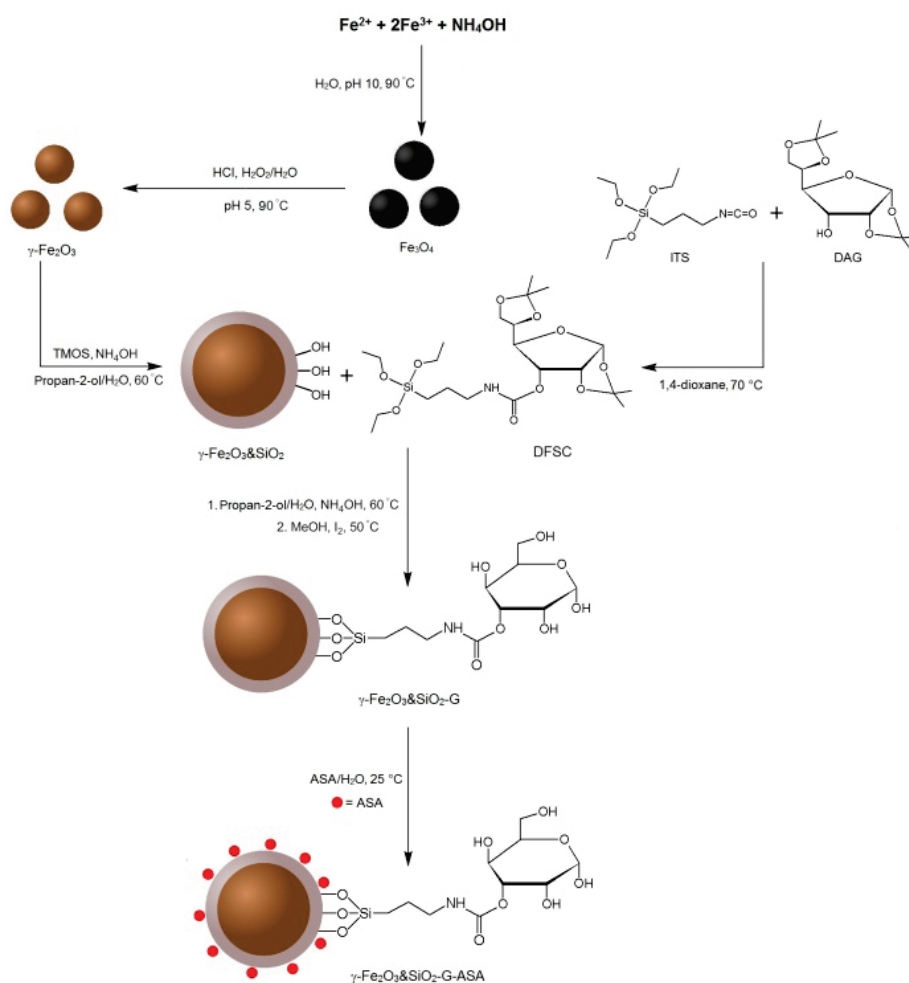
and moderately broad particle size distribution (PDI=1.3). Because the particles have to be dried before TEM imaging, they tend to form aggregates, however, the individual particles are still distinguishable on the micrographs and the particle size can be analyzed. As expected, the hydrodynamic particle size was substantially larger (D_h=64 nm) due to particle cluster formation in water; moreover, z-average diameter in DLS measurements is always $>D_n$. FT-Raman spectrum of the γ-Fe_2O_3 particles showed vibration bands at 560 and 1,090 cm⁻¹ attributed to the maghemite crystal lattice and surface hydroxyl groups, respectively (Fig. 3a).

Fig. 2. TEM micrographs of **a**) γ-Fe_2O_3, **b**) γ-Fe_2O_3&SiO_2 Run I/3, **c**) I/4, and **d**) I/6.

Fig. 3. FT-Raman spectra of **a**) γ-Fe_2O_3, **b**) γ-Fe_2O_3&SiO_2, **c**) γ-Fe_2O_3&SiO_2-DAG, **d**) γ-Fe_2O_3&SiO_2-G, and **e**) γ-Fe_2O_3&SiO_2-G-ASA nanopar-ticles.

Fig. 4. Synthesis of DFSC, -Fe₂O₃, γ-Fe₂O₃&SiO₂-G, and -Fe₂O₃&SiO₂-G-ASA nanoparticles. ITS - (3-isocyanatopropyl)triethoxysilane; DAG – diacetonide of D-glucose; TMOS – tetramethoxyorthosilicate; DFSC - 5-(2,2-dimethyl-1,3-dioxolan-4-yl)-2,2-dimethyltetrahydrofuro-[2,3-d][1,3]dioxol-6-yl (3-(triethoxysilyl)propyl)carbamate; ASA - ascorbic acid.

Surface modification of γ-Fe₂O₃ with SiO₂, DFSC, and ASA

(i) Surface of starting γ-Fe₂O₃ was modified with silica using TMOS as a precursor, which undergoes hydrolysis and condensation in alkaline medium (NH₄OH). Rather low TMOS/γ-Fe₂O₃ ratio (0.1 w/w) was applied to produce a thin SiO₂ shell (~1 nm). Presence of silica coating on the γ-Fe₂O₃&SiO₂ particles Run I/1 (Table 1) was confirmed by TEM, as well as by FT Raman spectrum (Fig. 3b), where a new vibration peak typical for silicates was observed at 180 cm⁻¹.

(ii) Surface of the nanoparticles Run I/1 was modified with DFSC obtained from ITS and DAG (Fig. 4). DFSC contains D-glucose (G), which increases stability of obtained composite particles in aqueous media. For preparation of γ-Fe₂O₃&SiO₂-G particles, DFSC/γ-Fe₂O₃&SiO₂ ratio was varied from 0.2 to 2 w/w (Table 1). The γ-Fe₂O₃&SiO₂-G particles Runs I/2-6 were 14-38 nm in size with PDI~1.3-1.6. With increasing DFSC/γ-Fe₂O₃&SiO₂ ratio, amount of D-glucose bound to the particles and thickness of γ-Fe₂O₃&SiO₂-G shell substantially increased from 1.7 to 11 wt.% and from 1 to

13 nm, respectively, as well as D_h increased up to ~250 nm (Table 1). DLS was used also to determine the particle size distribution. Polydispersity PI~0.25 of γ-Fe₂O₃&SiO₂-G nanoparticles Run I/3 obtained at optimal DFSC/γ-Fe₂O₃&SiO₂ ratio was in agreement with PDI values according to TEM characterizing moderately broad distribution. At high DFSC/γ-Fe₂O₃&SiO₂ ratio (Run I/6), however, neat silica-DAG spheres were formed (~100 nm in size) and particles tended to aggregate (Fig. 2d).

Successful modification was confirmed by FT-Raman spectroscopy, where presence of DFSC on the particles was documented by peaks at 200 and 1,085 cm⁻¹ corresponding to stretching deformations ν(Si-O-Si) and δ(Si-C), respectively, as well as peaks at 640 and 790 cm⁻¹ representing ring vibrations of DAG (Fig. 3c). Bands at 1,290 and 1,450 cm⁻¹ were ascribed to the ν(C-O-C) and ν(NH-CO) bond vibrations, respectively. Finally, strong signals at 2,930 and 2,990 cm⁻¹ were attributed to the ν_as(C-CH₃) vibrations of the double substituted semiacetal DAG cycles.

After the DAG cleavage, formation of glucose

Table 1. Characterization of γ-Fe$_2$O$_3$&SiO$_2$-G nanoparticles.

Run	DFSC/γ-Fe$_2$O$_3$&SiO$_2$ (w/w)	D_n (nm)	PDI	D_h (nm)	PI	ζ-potential (mV)	Bound glucose (wt.%)
I/1	0	13	1.28	126	0.24	42	0
I/2	0.1	14	1.34	94	0.23	36	1.7
I/3	0.2	16	1.32	82	0.25	35	3.0
I/4	0.5	20	1.42	109	0.30	36	4.6
I/5	1	26	1.48	168	0.37	35	7.7
I/6	2	38	1.62	253	0.46	33	11

DFSC - 5-(2,2-dimethyl-1,3-dioxolan-4-yl)-2,2-dimethyltetrahydrofuro[2,3-d][1,3]dioxol-6-yl (3-(triethoxysilyl)propyl)carbamate; D_n - number-average diameter (TEM); PDI - polydispersity index (TEM); D_h - hydrodynamic diameter (DLS); PI - polydispersity (DLS).

Table 2. Characterization of γ-Fe$_2$O$_3$&SiO$_2$-G-ASA nanoparticles originating from γ-Fe$_2$O$_3$&SiO$_2$-G Run I/3.

Run	ASA/γ-Fe$_2$O$_3$&SiO$_2$-G (w/w)	D_n (nm)	PDI	D_h (nm)	PI	ζ-potential (mV)	Bound ASA[a] (wt.%)	$A_{ROO\bullet}$ (mmol/g)	$A_{HO\bullet}$ (mmol/g)
II/1	0.1	18	1.34	68	0.23	-33	5.8	0.024	0.042
II/2	0.2	18	1.32	74	0.27	-37	9.1	0.084	0.103
II/3	0.5	19	1.28	79	0.22	-36	14.2	0.226	0.290
II/4	1	19	1.33	83	0.24	-42	21.1	0.887	1.05
II/5	2	20	1.30	86	0.29	-40	26.5	1.63	1.90
II/6	3	20	1.32	88	0.27	-46	28.9	2.31	2.70

ASA – ascorbic acid; D_n – number-average diameter (TEM); PDI – polydispersity index (TEM); D_h – hydrodynamic diameter (DLS); PI – polydispersity (DLS); $A_{ROO\bullet}$ and $A_{HO\bullet}$ – scavenging activity of peroxyl and hydroxyl radicals, respectively; [a]from C analysis.

was confirmed by presence of peaks at 661 and 704 cm^{-1} attributed to δ(C-O) wagging vibrations of CH-OH groups (Fig. 3d). Bands at 1,068 and 1,137 cm^{-1} were ascribed to stretching ν(C-O) of primary and secondary hydroxyl groups, respectively. Peak at 1,248 cm^{-1} documented presence of ν$_{as}$(C-O-C) stretching vibrations of ether oxygen bonds in glucose. Peak at 1,488 cm^{-1} was attributed to methylene group scissoring vibrations δ(H-C-H). Also a strong peak at 420 cm^{-1} showed the δ(C-C) vibrations of the propyl chain.

(iii) γ-Fe$_2$O$_3$&SiO$_2$-G particles Run I/3 were used for investigation of ASA adsorption (Table 2). With increasing ASA/γ-Fe$_2$O$_3$&SiO$_2$-G ratio, both D_n and D_h of γ-Fe$_2$O$_3$&SiO$_2$-G-ASA slightly increased from 18 to 20 and from 68 to 88 nm, respectively, due to formation of a thin carbohydrate layer fixed to the SiO$_2$ surface; thick multimolecular layer was not produced. The γ-Fe$_2$O$_3$&SiO$_2$-G-ASA particle size distribution did not change (PDI~1.3).

To confirm presence of G and ASA on the γ-Fe$_2$O$_3$&SiO$_2$-G and γ-Fe$_2$O$_3$&SiO$_2$-G-ASA nanoparticle surface, the carbon content was analyzed. Percentage of adsorbed ASA was then calculated by comparing carbon amount found in DFSC, ASA, and modified particles (Table 1 and 2). With increasing ASA/γ-Fe$_2$O$_3$&SiO$_2$-G ratio, amount of adsorbed ASA increased up to ~29 wt.% reaching a plateau, which is typical for Langmuir adsorption (Masel 1996). This adsorption limit corresponds to saturation equilibrium of adsorbate and is equal to the highest possible surface occupation.

FT-Raman spectrum of the γ-Fe$_2$O$_3$&SiO$_2$-G-ASA Run II/5 had typical peaks at 628 and 1,028 cm^{-1} corresponding to the out-of-plane OH deformation and ring bend vibrations of ASA, respectively (Fig. 3e). Peaks at 819, 1,128, 1,667, and 2,919 cm^{-1} were ascribed to the stretching deformations of C-C, C-O-C, and C=C groups of the ASA carbon ring and CH stretching of the carbon chain, respectively. The FT-Raman spectra thus also demonstrated successful coating of the particle surface with G and ASA.

Finally, γ-Fe$_2$O$_3$&SiO$_2$-G-ASA free-radical scavenging activity in SBB buffer was spectrophotometrically determined (Poláková *et al.* 2015). SBB buffer was selected for these experiments as it prevents the particle agglomeration, in contrast to phosphate-buffered saline, where the particles aggregate due to high affinity of phosphate ions to iron oxides. Also Good's buffers were found unsuitable for ROS determination due to their reactivity with the radicals (Grady *et al.* 1988). During the investigation, ROO$^\bullet$ and HO$^\bullet$ radicals formed by decomposition of AAPH and H$_2$O$_2$, respectively, decreased fluorescence due to oxidation of fluorescein in the reaction mixture. With increasing ASA content in the γ-Fe$_2$O$_3$&SiO$_2$-G-ASA particles, saturation adsorption was reached and the scavenging activity dramatically increased, which can be explained by a high ASA diffusion from the particle surface in the liquid phase. Maximum scavenging activity was found in γ-Fe$_2$O$_3$&SiO$_2$-G-ASA nanoparticles Run II/6 (containing almost 30 wt.% ASA), which captured 2.3 and 2.7 mmol of ROO$^\bullet$ and HO$^\bullet$ per g, respectively (Table 2), while pure ASA captured ~11 mmol of both radicals/g.

Discussion

Fe$_3$O$_4$ nanoparticles were obtained by co-precipitation of iron salts in basic medium (Fig. 4), which is a relatively easy and versatile method of iron oxide synthesis (Massart 1981). Several reaction parameters are crucial for formation of stable colloids with a relatively narrow particle size distribution, such as Fe^{2+}/Fe^{3+} ratio=2 mol/mol, type of the salt (chloride, nitrate, sulfate), amount of precipitating base, temperature, pH, stirring speed, etc. In this report, Fe chlorides and ammonia were preferred reactants used at temperatures 70 and 90 °C. To obtain γ-Fe$_2$O$_3$, which is more oxidatively stable than Fe$_3$O$_4$ due to the absence of Fe^{2+} ions, hydrogen peroxide was used as a strong oxidation agent, which does not produce undesirable byproducts. Oxidant/magnetite ratio, pH, temperature, reaction time, as well as subsequent washing and sonication, play an important role in preparation of a high-quality product.

To enhance the radical scavenging ability and to avoid oxidative stress caused by traces of Fe^{2+} ions leaching from the γ-Fe$_2$O$_3$ particles, their surface was coated with silica, D-glucose, and finally modified with ASA; resulting nanoparticles were termed as γ-Fe$_2$O$_3$&SiO$_2$-G-ASA (Fig. 4). It is interesting to note

that D_h of initial γ-Fe$_2$O$_3$&SiO$_2$ particles (126 nm) decreased after reaction with DFSC at DFSC/γ-Fe$_2$O$_3$&SiO$_2$=0.1 and 0.2 w/w to 94 and 82 nm, respectively. This is ascribed to decreased particle clustering during DLS measurements due steric repulsion of D-glucose attached to the particles. D-glucose can be thus considered as an excellent hydrophilic modification agent inducing high colloidal stability of the particles. The γ-Fe$_2$O$_3$&SiO$_2$-G particles Run I/3 were then used in the final ASA adsorption experiments. With DFSC/γ-Fe$_2$O$_3$&SiO$_2$ ratio >0.2 w/w, glucose-modified silica shell thickness increased and induced particle aggregation in water. As a result, D_h of γ-Fe$_2$O$_3$&SiO$_2$-G nanoparticles Run I/4-6 was substantially larger than in Run I/2 and I/3. As expected hydrodynamic particle diameter was always larger than the size from TEM, which measures particles in dry state, where carbohydrate moieties are in a collapsed state. While γ-Fe$_2$O$_3$&SiO$_2$ and γ-Fe$_2$O$_3$&SiO$_2$-G particles had a positive charge (*ca.* 35 mV), ASA (due to presence of acidic hydroxyl groups) introduced negative charges on the surface, absolute value of which increased from 33 to 46 mV with increasing ASA/γ-Fe$_2$O$_3$&SiO$_2$-G ratio. Since it is well-known that absolute values of ζ-potential >30 mV render the particles with colloid stability (Babič *et al.* 2009), there is no surprise that the γ-Fe$_2$O$_3$&SiO$_2$-G-ASA particles Run II did not exhibit any tendency to aggregation. However, as expected, each modification step increased the particle size.

Conclusions

The γ-Fe$_2$O$_3$&SiO$_2$-G-ASA nanoparticles demonstrated remarkable free-radical scavenging activity, which reached 70 % of that for pure ASA. Such nanoparticles, combining both magnetic targetability and antioxidative activity, can in future undoubtedly find new biomedical applications, in particular, for treatment of fatal disorders, such are cardiovascular and neurodegenerative diseases and cancer.

Conflict of Interest

There is no conflict of interest.

Acknowledgements

References

BABIČ M, HORÁK D, JENDELOVÁ P, GLOGAROVÁ K, HERYNEK V, TRCHOVÁ M, LIKAVČANOVÁ K, HÁJEK M, SYKOVÁ E: Poly(*N,N*-dimethylacrylamide)-coated maghemite nanoparticles for stem cell labeling. *Bioconjug Chem* **20**: 283-294, 2009.

BABIČ M, HORÁK D, TRCHOVÁ M, JENDELOVÁ P, GLOGAROVÁ K, LESNÝ P, HERYNEK V, HÁJEK M, SYKOVÁ E: Poly(*L*-lysine)-modified iron oxide nanoparticles for stem cell labeling. *Bioconjugate Chem* **19**: 740-750, 2008.

BULTE JWM, KRAITCHMAN DL: Iron oxide MR contrast agents for molecular and cellular imaging. *NMR Biomed* **17**: 484-499, 2004.

DORNIANI D, HUSSEIN MZB, KURA AU, FAKURAZI S, SHAARI AH, AHMAD Z: Preparation of Fe_3O_4 magnetic nanoparticles coated with gallic acid for drug delivery. *Int J Nanomed* **7**: 5745-5756, 2012.

FERRUCCI JT, STARK DD: Iron oxide-enhanced MR imaging of the liver and spleen. *Am J Roentgenol* **155**: 943-950, 1990.

GEETHA K, RAGHAVAN MSS, KULSHRESHTHA SK, SASIKALA R, RAO CP: Transition-metal saccharide chemistry: Synthesis, spectroscopy, electrochemistry and magnetic susceptibility studies of iron(III) complexes of mono- and disaccharides. *Carbohydrate Res* **271**: 163-175, 1995.

GILDERSLEEVE JC, OYELARAN O, SIMPSON JT, ALLRED B: Improved procedure for direct coupling of carbohydrates to proteins via reductive amination. *Bioconjug Chem* **19**: 1485-1490, 2008.

GRADY JK, CHASTEEN ND, HARRIS DC: Radicals from "Good's" buffers. *Analyt Biochem* **173**: 111-115, 1988.

IFFAT AT, MAQSOOD ZT, FATIMA N: Study of complex formation of Fe (III) with tannic acid. *J Pak Chem Soc* **27**: 174-177, 2005.

KAMAT M, EL-BOUBBOU K, ZHU DC, LANSDELL T, LU X, LI W, HUANG X: Hyaluronic acid immobilized magnetic nanoparticles for active targeting and imaging of macrophages. *Bioconjug Chem* **21**: 2128-2135, 2010.

KEKKONEN V, LAFRENIERE N, EBARA M, SAITO A, SAWA Y, NARAIN R: Synthesis and characterization of biocompatible magnetic glyconanoparticles. *J Magn Magn Mater* **321**: 1393-1396, 2009.

KRAEMER SM: Iron oxide dissolution and solubility in the presence of siderophores. *Aquat Sci* **66**: 3-18, 2004.

LEMIEUX GA, BERTOZZI CR: Chemoselective ligation reactions with proteins, oligosaccharides and cells. *Trends Biotech* **16**: 506-513, 1998.

LU Y, YIN Y, MAYERS BT, XIA Y: Modifying the surface properties of superparamagnetic iron oxide nanoparticles through a sol-gel approach. *Nano Lett* **2**: 183-186, 2002.

MASEL R: Langmuir adsorption model. In: *Principles of Adsorption and Reaction on Solid Surfaces*. Wiley-Interscience, New York, 1996, pp 239-244.

MASSART R: Preparation of aqueous magnetic liquids in alkaline and acidic media. *IEEE Trans Magn* **17**: 1247-1248, 1981.

OLDEN K, PARENT JB, WHITE SL: Carbohydrate moieties of glycoproteins; a re-evaluation of their function. *Biochim Biophys Acta* **650**: 209-232, 1982.

PATSULA V, MOSKVIN M, DUTZ S, HORÁK D: Size-dependent magnetic properties of iron oxide nanoparticles. *J Phys Chem Solids* **88**: 24-30, 2016.

PLUG CM, DECKER D, BULT A: Complex stability of ferrous ascorbate in aqueous solution and its significance for iron absorption. *Pharm Weekblad* **16**: 245-248, 1984.

POLÁKOVÁ L, RAUS V, KOSTKA L, BRAUNOVÁ A, PILAŘ J, LOBAZ V, PÁNEK J, SEDLÁKOVA Z: Antioxidant properties of 2-hydroxyethyl methacrylate-based copolymers with incorporated sterically hindered amine. *Biomacromolecules* **16**: 2726-2734, 2015.

ROQUE ACA, BICHO A, BATALHA IL, CARDOSO AS, HUSSAIN A: Biocompatible and bioactive gum Arabic coated iron oxide magnetic nanoparticles. *J Biotech* **144**: 313-320, 2009.

SUN YK, MA M, ZHANG Y, GU N: Synthesis of nanometer-size maghemite particles from magnetite. *Colloids Surf* **245**: 15-19, 2004.

WANG YX: Superparamagnetic iron oxide based MRI contrast agents: Current status of clinical application. *Quant Imaging Med Surg* **1**: 35-40, 2011.

WILHELM C, BILLOTEY C, ROGER J, PONS JN, BACRI JC, GAZEAU F: Intracellular uptake of anionic superparamagnetic nanoparticles as a function of their surface coating. *Biomaterials* **24**: 1001-1011, 2003.

WINTERBOURN CC: Toxicity of iron and hydrogen peroxide: The Fenton reaction. *Toxicol Lett* **82**: 969-974, 1995.

WUST P, GNEVECKOW U, JOHANNSEN M, BÖHMER D, HENKEL T, KAHMANN F, SEHOULI J, FELIX R, RICKE J, JORDAN A: Magnetic nanoparticles for interstitial thermotherapy – feasibility, tolerance and achieved temperatures. *Int J Hyperthermia* **22**: 673-685, 2006.